OPEN ACCESS
IOP Publishing
Journal of Micromechanics and Microengineering
J. Micromech. Microeng. **35** (2025) 055001 (17pp)
https://doi.org/10.1088/1361-6439/adc9bb

Alignment teaching assisted fully automated mechanical dicing of MEMS and NEMS devices

Muhammad Rashid Mahmood[1,3], Jens Griesmann[2], Sotir Chervenkov[2] and Mehmet Yilmaz[3,*]

[1] Institute of Materials Science and Nanotechnology, Bilkent University, 06800 Ankara, Turkey
[2] DISCO Hi-TEC EUROPE GmbH, Liebigstrasse 8, Kirchheim b. Muenchen, D-85551, Germany
[3] National Nanotechnology Research Center (UNAM), Bilkent University, 06800 Ankara, Turkey

E-mail: mehmetyilmaz@unam.bilkent.edu.tr

Received 18 October 2024, revised 25 March 2025
Accepted for publication 7 April 2025
Published 22 April 2025

Abstract

In the dynamic landscape of semiconductor manufacturing, the demand for innovative and efficient techniques is ever-growing. Dicing is a singulation process where a machine known as a dicing saw or dicer uses a diamond blade or laser to separate dies from a wafer through a manual, semi-automated, or fully automated process. In diamond blade or mechanical dicing, the dicing saw utilizes a thin blade to cut through a wafer. This paper presents the design and implementation of an alignment teaching-assisted fully automated dicing process for the singulation of microelectromechanical systems (MEMS) devices. A pseudo-MEMS device with potential alignment targets was designed and manufactured by conventional microfabrication techniques. Alignment teaching operation was optimized for the dicing saw by finding the most appropriate alignment targets, as alignment teaching is as a pre-requisite for realizing both auto-alignment and automated dicing processes. A systematic trial-and-error approach was employed to discover the most suitable alignment targets from a pool of twenty-three potential target patterns. A circle was identified as an excellent macro target, while the addition symbol, hash symbol, and rectangle-pair were determined to be the most appropriate micro targets. The developed versatile singulation process is capable of executing an alignment teaching assisted fully automated (i.e. a total of one-click to initiate and finalize) dicing for singulating MEMS device chips, irrespective of alignment target color, die size, or wafer material. Furthermore, we developed, and experimentally validated, a mathematical model to estimate the total process time for the automated dicing.

* Author to whom any correspondence should be addressed.

Original Content from this work may be used under the terms of the Creative Commons Attribution 4.0 licence. Any further distribution of this work must maintain attribution to the author(s) and the title of the work, journal citation and DOI.

© 2025 The Author(s). Published by IOP Publishing Ltd

Supplementary material for this article is available online

Keywords: diamond blade dicing, MEMS, alignment target, alignment teaching, automated dicing, dicing time

1. Introduction

The safe transition from wafer-level (i.e. an array of multiple microelectromechanical systems (MEMS) devices) to die-level (i.e. single MEMS device) chips is a crucial step, given the delicate nature of the structures of MEMS or NEMS devices [1]. A dicing machine is capable of doing this safe transition of the devices through semi-automated or fully automated dicing procedures. Mechanical or diamond blade dicing is more prevalent in the device singulation industry than laser dicing due to many factors. Traditional mechanical or diamond blade cutting remains significant in device singulation because of its ability to work with a variety of materials, cost efficiency, mass production, cut-edge quality, and minimal thermal effects. Laser dicing provides contactless processing and high precision; however, it leads to severe thermal damage and decreased die strength [2].

The size of integrated circuits is getting smaller as technology develops, allowing manufacturers to produce MEMS and NEMS devices that are smaller and lighter yet having higher speed, power dissipation, and accuracy [3]. Consequently, precise and high throughput singulation processes are essential for isolating individual chips from wafers. The fully automated dicing method reduces the energy consumption and processing time of the tool, enhances the manufacturing rates of MEMS or NEMS chips, and expedites device packaging procedures. In addition, the likelihood of wrong-cutting due to human error in completely automated dicing is substantially lower in comparison to semi-automated or manual dicing processes.

This paper is the first to introduce alignment-teaching-assisted fully automated mechanical dicing in the literature. During the automated dicing, the dicing saw automatically aligns the wafer and dices it into chips (by identifying the number of required cut lines) with a single button press. Auto-alignment is a pre-requisite for automated dicing, and alignment teaching is the pre-requisite for the auto-alignment of the wafer. Conducting the alignment teaching operation requires the most appropriate macro and micro alignment targets on the devices of the wafer to be singulated. The dicing saw (DISCO DAD3220) records the alignment teaching data utilizing a single macro and a single micro-target. However, the latest versions of dicing machines provide the option to use two macro-targets and two micro-target patterns for the execution of alignment teaching operations.

A layout editor software is used to design wafer-scale square pseudo-MEMS devices with dimensions of 16.75 mm by 16.75 mm. Twenty-three potential alignment targets are created on the vacant spaces of each pseudo-MEMS chip on a 4 inch wafer. The circular, rectangular, and square targets serve as macro alignment targets, whilst features with addition symbol, hash symbol, and rectangle pair are created as micro targets. The dicing saw utilizes macro targets for coarse alignment and micro-targets for precise alignment of the wafer. Borosilicate glass (Pyrex-7740) and silicon wafers are used as substrates for device fabrication because of their widespread use in the microfabrication industry to produce MEMS and NEMS devices [4]. Conventional micro and nanofabrication techniques, including photolithography, metal deposition, and lift-off, are used to produce the pseudo-MEMS devices (details are explained in section 2).

Each prospective alignment target on the pseudo-MEMS chip undergoes an alignment teaching operation to identify the most appropriate macro and micro targets via a systematic trial-and-error approach. The findings from alignment teaching trials indicate that the circles are the optimal macro targets, whereas addition symbols, hash symbols, and rectangle pairs are considered excellent micro targets. Following that, the optimized alignment targets (macro and micro) are recorded in the dicing machine to complete the alignment teaching operation. Finally, the square MEMS chips on the wafer are singulated utilizing a two-channel alignment-teaching-assisted fully automated dicing process. Hexagonal or octagonal dies may be singulated using a 3-channel or 4-channel dicing operation, respectively. Therefore, a process recipe for completely automated dicing has been developed.

Guenther *et al* describe employing automated dicing to create mesa structures for their devices. However, alignment teaching and teaching-assisted automatic dicing are not explained [5]. Mei *et al* highlight completely automated dicing operation but do not provide specific information on the process details for alignment teaching or automated dicing [6]. Although Basu *et al* used a dicing saw to cut a substrate accurately into samples with specified dimensions, the study lacks an explanation of how the automated dicing procedure was carried out [7]. Richard *et al* used the DISCO DAD361 dicing saw machine equipped with a 30 um wide diamond blade to fabricate trench-like structures. Nonetheless, this research lacks information on the use of alignment teaching-assisted automatic dicing [8]. The diamond blade dicing saw (DISCO DAD321) was utilized in several scientific studies without delving into the details of alignment teaching operation or automated dicing [9–25]. The literature survey highlights the absence of information on alignment teaching and fully automated mechanical dicing procedures, and we aim to contribute to filling this technological knowledge gap.

The last part of the article focuses on developing mathematical formulations for precise and detailed calculations of the total dicing saw processing time for the chip singulation from manufactured wafers. An approximate formula and dicing time simulator based on analytical formulations to calculate the total dicing saw processing time for a given wafer is developed [26]. Furthermore, an analytical method for the calculation of the total dicing distance and total wafer-cutting time by calculating the total cutting length of the wafer is developed [27]. However, neither of the two calculation approaches took into account the details of turnover time for each cut nor the additional time that is required for multi-step cutting instead of a single-step cutting process, requiring the development of more precise and comprehensive analytical solutions.

This article is organized as follows: section 1 includes a literature overview on alignment teaching assisted fully automated mechanical dicing of MEMS and NEMS devices. Section 2 discusses the whole microfabrication process for manufacturing wafer-scale pseudo-MEMS device chips. Optimization of the alignment teaching process via selection of most suitable alignment targets is presented in section 3. Section 4 explains how to feed the selected alignment target into the dicing saw using alignment teaching and potential errors and their troubleshooting. Section 5 provides information on the implementation of alignment teaching assisted fully automated dicing of 4 inch wafers. The mathematical formulations for calculating the processing time required for the mechanical dicing of MEMS and NEMS devices are given in section 6. Section 7 presents a discussion and analysis of the research findings. Section 8 provides a conclusion and future directions for the work that has been completed.

2. The design and fabrication of pseudo-MEMS devices

A fabrication mask was designed to manufacture pseudo-MEMS devices for automated dicing saw processing studies. On the vacant spaces of a 16.75 mm $\times$ 16.75 mm pseudo-MEMS device, a total of 23 potential alignment targets (also called target patterns) were created using layout editor software. The 4 $\times$ 4 array of pseudo-MEMS devices was designed primarily to demonstrate the wafer-scale automated dicing process. The target patterns of various geometries and dimensions were created with careful consideration of their design criteria: 1. The macro target should be a simple figure (i.e. less affected by $\pm$5 degrees of theta rotation), while the micro-target must contain multiple straight lines in the *Y*-direction and at least one straight line in the *X*-direction, 2. Macro and micro targets should have high contrast compared to their background, and both targets should bear no similar figure in the same die (i.e. they must have a unique shape) [28]. Fifteen out of twenty-three circular, square, and rectangular features were drawn as potential macro targets, while the remaining eight features with addition symbol, hash symbol, and the rectangle pair were designed as potential micro targets. Figure 1 shows a pseudo-MEMS device chip featuring potential alignment targets labeled with identification numbers ranging from 1 to 23.

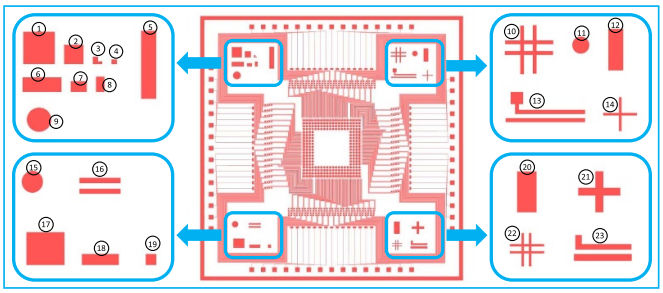

Figure 1. Chip-scale drawing of a 16.75 mm by 16.75 mm pseudo-MEMS device chip with 23 potential alignment targets: 15 Macro Targets and 8 Micro Targets.

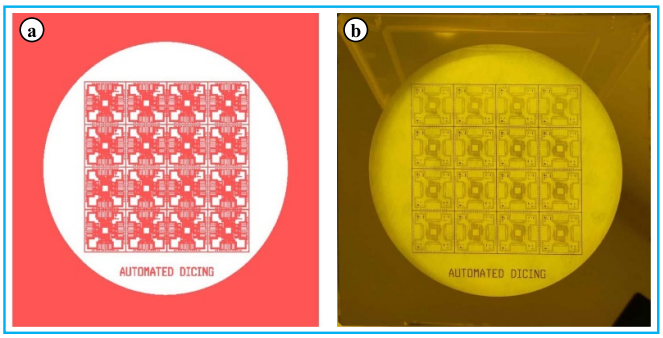

Figure 2. Photomask (5 in $\times$ 5 in) for wafer-scale manufacturing of pseudo-MEMS device chips: (a) Photomask design, (b) Manufactured photomask.

A 5 inch by 5 inch soda lime glass mask covered with photoresist was first exposed using a laser mask writer (DWL-66FS, Heidelberg) to manufacture a photomask. The photoresist underwent development, followed by a wet-etching process of the chrome layer on the glass mask in order to get the desired pattern. Finally, the patterned mask photoresist was removed from the photomask. The photomask created for the photolithography process is shown in figure 2.

Borosilicate glass (Pyrex-7740) and silicon wafers underwent the photolithography procedure alone to achieve pseudo-MEMS devices with photoresist features on their surfaces. Both wafers were spin-coated with a 1.98-micron thick layer of positive tone photoresist AZ 5214E. The photoresist was pre-baked by putting the wafers on a hot plate for about 50 s. Following that, the wafers underwent exposure with ultraviolet dosage of 30 mJ.cm^{-2} after positioning the photomask to the mask aligner. Finally, the photoresist on the wafers was developed with a diluted solution of AZ 400 K developer. Figure 3 shows the fabricated wafers.

Pyrex and silicon wafers also underwent a series of processes, including photolithography, metal deposition, and lift-off, to create copper structures on the surface of pseudo-MEMS devices. A 1.98-micron thick layer of AZ 5214E photoresist was applied to the wafers using a spin-coating process, which is a negative tone photoresist with image reversal and was used for improved lift-off processing. The photoresist

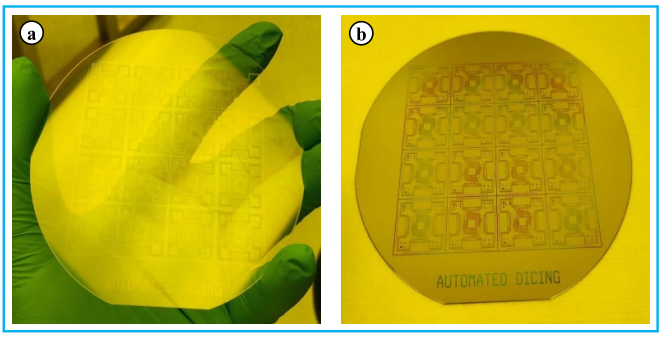

Figure 3. Four-inch diameter wafers with pseudo-MEMS devices having photoresist features: (a) Pyrex-7740 wafer, (b) Silicon wafer.

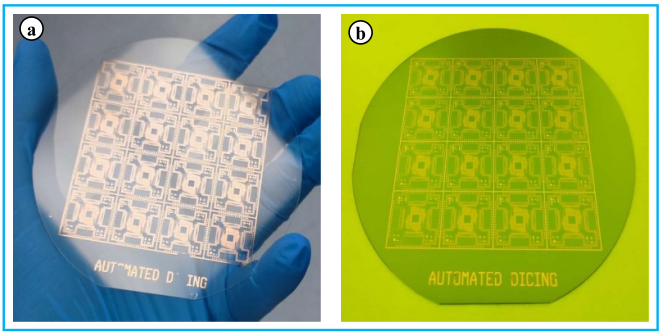

Figure 4. Four-inch diameter wafers with pseudo-MEMS devices having copper features: (a) Pyrex-7740 wafer, (b) Silicon wafer.

was subjected to soft-baking on a hot plate for about 50 s. Following that, the wafers were exposed (1st exposure) to an ultraviolet dosage of 30 mJ.cm^{-2} after positioning the photomask to the mask aligner. The photoresist was subjected to post-exposure reversal baking by putting the wafers on a hot plate set at a temperature of 120 °C for 2 min. Next, the wafers covered with photoresist were flood-exposed to ultraviolet light with a dosage of 300 mJ·cm^{-2} (2nd exposure). The photoresist was developed using a diluted solution of AZ 400 K developer. The e-beam evaporator was used to produce a copper layer on wafers that was 50 nm thick. Lastly, the wafers were submerged in pure acetone until the photoresist was lifted off. The wafers with copper features are showed in figure 4.

3. Selection of appropriate targets for alignment teaching

Selecting a unique alignment target is essential for an effective teaching alignment procedure. The alignment target should have little resemblance to neighboring features on the device or, ideally, no similarity. Suitable alignment targets are a prerequisite for a successful alignment teaching operation. During auto-alignment, the macro targets are responsible for the rough alignment, whilst the micro targets are responsible for the more precise fine alignment. An alignment teaching was conducted for each prospective alignment target to determine the most suitable one, and the dicing saw tool determined the suitability of the alignment targets based on the Q values of the alignment targets. The Q value is a number in percentage that defines how much the detected alignment target on the substrate resembles the target recorded in the dicing saw, and Q value is based on the contrast of the image captured by the machine. The Pyrex and Silicon wafers with pseudo-MEMS devices having photoresist or copper features were used for these studies.

3.1. Macro target selection

Each chip has 15 potential macro targets out of 23 total alignment targets shown in figure 1. Potential macro targets were selected based on the design criteria explained in section 2, and alignment teaching was conducted on each macro target because of its distinct geometry and dimensions to find the optimal alignment target. The dicing saw performed three verification checks to evaluate the suitability of the target, depending on the Q-values obtained from the verification process.

3.1.1. Spiral check. Once the potential macro target was selected, the dicing saw performed a spiral check to ensure the uniqueness of the selected macro target and to confirm that there were no similar targets (or features) present in the same chip. The microscope of the dicing saw scanned the chip in a spiral pattern, starting at the position of the macro target. An acceptable macro target should possess a Q-value below 60%, the difference between Q-level and spiral check Q-margin. The Q-value for the spiral check was set to a maximum of 60% threshold to rule out the possibility of mis-recognition of the selected alignment target in case it exhibits high resemblance (i.e. high Q-value) with other identical features on the MEMS chip. Based on this criterion, the dicing saw rejects the selected alignment target having 60% or more resemblance with any other feature of the chip, and the machine recommends selecting another unique target with less resemblance.

The mean Q-values for the 11 macro targets were below 60%, suggesting they are suitable for alignment teaching work. Nevertheless, the dicing machine rejected macro targets with identification numbers 4, 7, 12, and 19 because of their resemblance to adjacent features on the MEMS chip. Table 1 summarizes the outcomes of the spiral check.

3.1.2. Angle check. The purpose of this verification check is to rectify any considerable tilt of the wafer during auto-alignment, which may occur during sample preparation. The dicing saw purposely tilted the workpiece by up to ±5° and attempted to identify the same target pattern inside the same die after rotating. An acceptable macro target must maintain a Q-value above the Q-level threshold (80%), meaning the identified and recorded targets should exhibit maximum similarity.

The rationale behind setting the Q-level threshold to 80% for the detected alignment target was to provide a tolerance of 20%, as the detected alignment mark will not show 100% resemblance with the recorded target due to inevitable fabrication defects and dimensional variations in the device features

Table 1. Q-value results of 15 potential macro targets having distinct geometries and dimensions.

Macro target details			Mean Q-values (in percentage)		
ID no.	Shape	Dimensions (in microns)	Spiral check	Angle check	Index check
1	Rectangle	Length * width = 650 * 675	40.4	51.5	99
2	Square	Length * width = 400 * 400	37.5	74	99
4	Rectangle	Length * width = 110 * 90	Resembles other features on the chip.		
5	Rectangle	Length * width = 308 * 1420	37.4	40	99
6	Rectangle	Length * width = 800 * 300	34.8	56	99
7	Rectangle	Length * width = 325 * 215	Resembles other features on the chip.		
8	Rectangle	Length * width = 170 * 312	45.7	86.5	99
9	Circle	Radius = 250	32.8	97	99
11	Circle	Radius = 175	47.9	96.5	99
12	Rectangle	Length * width = 305 * 850	Resembles other features on the chip.		
15	Circle	Radius = 200	33.4	96.5	99
17	Rectangle	Length * width = 720 * 600	40.4	63	99
18	Rectangle	Length * width = 700 * 200	36.8	55	99
19	Square	Length * width = 200 * 200	Resembles other features on the chip.		
20	Rectangle	Length * width = 365 * 790	38.6	62	98

(i.e. alignment targets). Furthermore, the Q-level threshold is not a fixed number and can be increased to 85% or 90% by reducing tolerance to 15% or 10%, respectively, provided that one has an optimum cleanroom fabrication process with minimal defects or variations. From the other side, setting the Q-value below 80% may result in mis-recognition of alignment targets with other features on the chip having comparable Q-values, causing alignment errors. The macro targets 1, 2, 5, 6, 17, 18, and 20 showed average Q-values of 51.5%, 74%, 40%, 56%, 63%, 55%, and 62%, respectively, after the angle check. These results indicate that these targets are not appropriate for the alignment teaching. Conversely, the dicing machine recognized targets 8, 9, 11, and 15 as suitable macro targets due to their Q-values above 80%. The Q-value outcomes of the angle verification are shown in table 1.

3.1.3. Index check. In order to determine whether the neighboring chip has the same macro target, the dicing saw moved one index to the right on the wafer and performed an index check. The Q-value must be above the Q-level requirement of 80% for the macro target to be acceptable. Ideally, the detected alignment target should perfectly resemble (i.e. 100% Q-value) the target recorded in the dicing saw. However, the Q-level threshold is set to 80% for the detected alignment target, allowing for a 20% tolerance since it will not exhibit 100% similarity with the recorded target due to unavoidable cleanroom fabrication defects and dimensional variations in the device features (i.e. alignment targets).

Based on the statistical data shown in table 1, it was observed that 11 out of 15 potential macro targets achieved Q-values over 98%. This indicates that these targets are suitable for alignment teaching.

3.1.4. Macro target selection results. The dicing saw rejected 11 potential macro target patterns that were not suitable for alignment teaching work based on the outcomes of the three verification checks. Figure 5 illustrates that 3 circular targets and 1 rectangular target had the greatest Q-values in angle and index checks, whereas they had the lowest values in spiral checks compared to the other targets.

3.2. Micro target selection

Alignment teaching was also conducted on 8 potential micro targets in sequential order to choose the optimal alignment target. The dicing saw performed two verification tests to

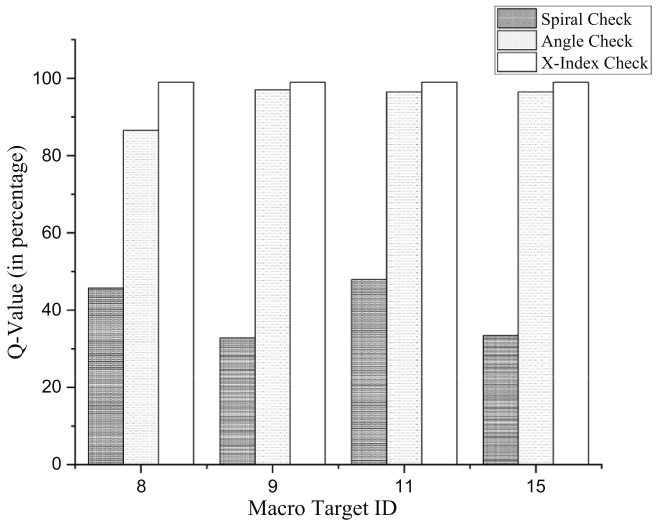

Figure 5. *Q*-value outcomes of the 4 approved macro targets.

Table 2. *Q*-value results of 8 potential micro targets having distinct geometries and dimensions.

Micro target details			Mean *Q*-values (in percentage)	
ID no.	Shape	Dimensions (in microns)	Spiral check	Index check
3	Polygon	Edge lengths = 148*190*47*90	34.25	98.5
10	Hash symbol	Arm thickness = 75	43.57	98.5
13	Rectangle-pair	Width of one bar = 80	30	99
14	Addition symbol	Arm thickness = 50	41.75	99
16	Rectangle-pair	Width of one bar = 95	45.75	97.25
21	Addition symbol	Arm thickness = 150	29.5	98.75
22	Hash symbol	Arm thickness = 40	46	98.5
23	Rectangle-pair	Width of one bar = 130	56	97.25

determine the suitability of the selected target pattern. The dicing saw does not perform an angle check during micro target teaching, as the angular deviation of the wafer is already resolved during the macro target teaching process. The micro target teaching focuses on smaller alignment marks for fine alignment (relative to other features on the chip) rather than adjusting the global positioning or angle of the entire wafer.

3.2.1. Spiral check. The dicing saw performed a spiral check in 9 separate view fields at a high magnification of 7.5X to verify the absence of any identical micro targets. The microscope camera provides a high-magnification view field of 640 microns by 640 microns. A micro-target with a *Q*-value below 60% is considered acceptable since it shows less resemblance with other chip features. The *Q*-value for the spiral check was set to a maximum of 60% threshold to rule out the possibility of mis-recognition of the selected alignment target with other chip features having a high similarity index (i.e. high *Q*-value) with the chosen target. Based on this criterion, the dicing saw rejects the selected alignment target exhibiting 60% or more resemblance with other features on the chip, and the machine recommends selecting another unique alignment target with a lower similarity index or resemblance with the chip features (i.e. low *Q*-value).

Each of the 8 potential micro targets had *Q*-values lower than the 60% threshold, with target 23 boosting the highest *Q* value of 56%. The results of the spiral check's *Q*-values are shown in table 2.

3.2.2. Index check. The microscope of the dicing saw moved along the *Y*-axis and *X*-axis to detect the chosen micro target on 8 additional dies or chips. The tool used the index values (or the chip dimensions) included in the device data to move to the other chips. The *Q*-value must be above the 80% threshold to be considered an acceptable micro target. The *Q*-level threshold is set to 80% (similar to the macro target selection criterion in section 3.1.3) for the detected alignment target, allowing for a 20% tolerance since it will not exhibit 100% similarity with the recorded target due to inevitable fabrication defects and dimensional variations in the device features (i.e. alignment targets).

In this verification test, all 8 micro targets exhibited *Q*-values over 97%, indicating their suitability for alignment teaching. Table 2 shows the *Q*-values for the index check of the micro targets.

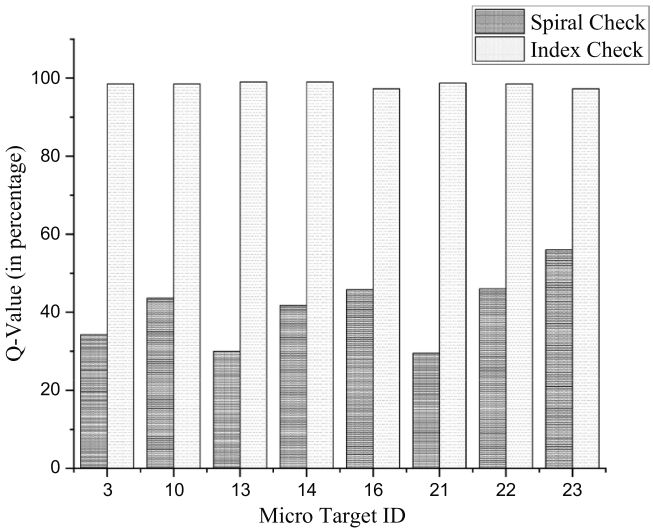

Figure 6. Q-values of the 8 approved micro targets.

3.2.3. Micro target selection results. The potential micro targets, including the hash symbol, addition symbol, and rectangle-pair, all qualify as appropriate micro targets in alignment teaching trials, as seen in figure 6.

4. Alignment teaching procedure

The alignment teaching process starts with sample preparation and ends with recording teaching data (macro and micro targets) in the dicing saw. Figure 7 illustrates the process flow steps involved in dicing a wafer, which includes alignment teaching, auto alignment, and fully automated dicing.

4.1. Sample preparation

Establishing a reliable alignment-teaching procedure begins with properly preparing the samples. The dicing frame was first attached to the adhesive side of the dicing tape (D-841), with the monogram of the dicing frame (DISCO) positioned towards the user and facing upwards. The 4 inch wafer was attached to the frame by aligning their midpoints manually. The air trapped between the dicing tape and the wafers was removed by positioning it on the vacuum-engaged chuck table of the dicing saw for roughly 30 minutes. The vacuuming feature of the chuck table and the permeable material of the dicing tape allowed the elimination of the air pockets. Figure 8 shows a prepared sample.

4.2. Device data preparation

The dimensions of the workpiece and the dicing tape were recorded on the 'Device Data' screen, including their size, shape, and thickness. The Y-index (equivalent to width of the chip), the workpiece's feed rate, the blade height (from the chuck table), and the blade RPM were also entered as cutting parameters. The dicing quality of MEMS/NEMS chips (i.e. obtaining 90-degree side-walls, and/or smaller and fewer edge chipping damages) can be improved by optimizing the cutting parameters such as blade RPM (revolutions per minute) and feed rate [29]. The 'Measure' feature on the device data screen enables the finding of real index values. The angle between channel CH1 and channel CH2 was kept at 90 degrees because of the square MEMS chips. Figure 9 shows a screenshot of the device data.

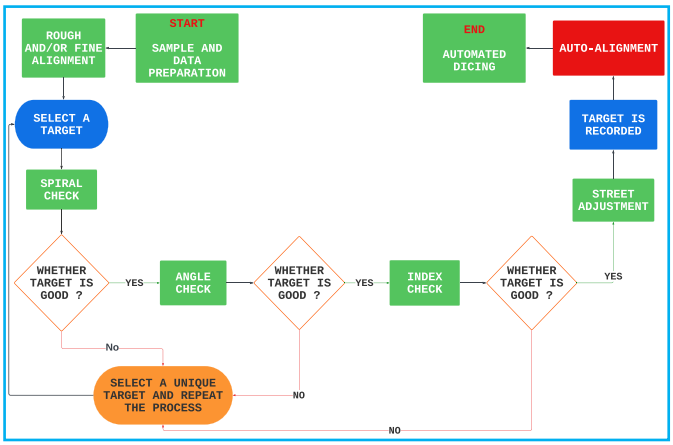

Figure 7. Process flow diagram: alignment teaching to automated dicing.

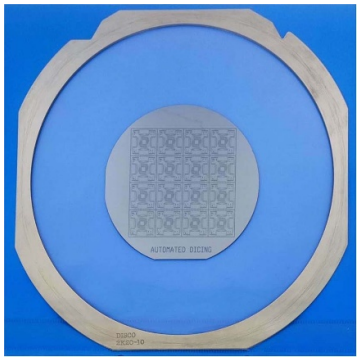

Figure 8. Four-inch diameter Silicon wafer mounted on a dicing frame prepared for alignment teaching and fully automated dicing.

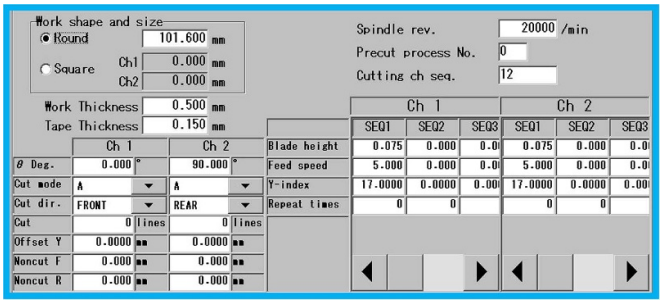

Figure 9. Screenshot of device data dicing saw showing the workpiece dimensions and cutting parameters.

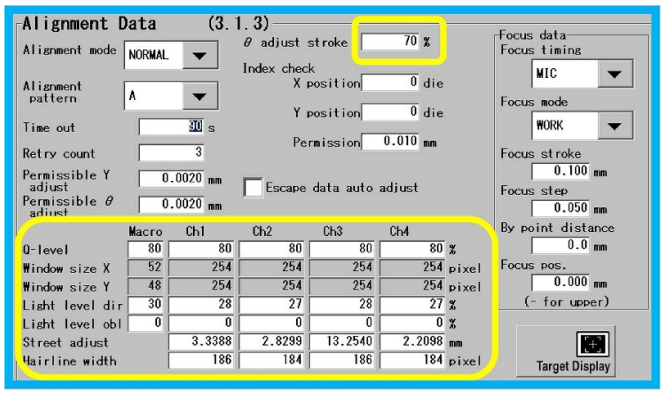

Figure 10. Screenshot of dicing saw showing the alignment teaching data.

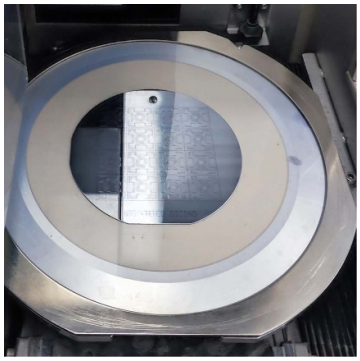

Figure 11. Four-inch diameter Silicon wafer positioned on the chuck table of the dicing saw.

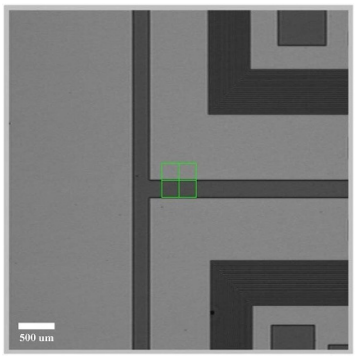

Figure 12. Screenshot of the dicing saw after the target window was aligned horizontally with the dicing street edge on the wafer at low magnification (0.75X).

4.3. Alignment data preparation

The Q-value: The dicing saw determines whether the recorded and detected targets are similar by comparing their images during the alignment teaching and auto-alignment operations. The Q value, with an overall magnitude of 100, indicates the degree of similarity between the images of the detected target pattern and the recorded target pattern.

The Q-Level: The minimum threshold Q-value (or the Q-level) for an acceptable target pattern for angle and index verification checks was set to 80% in the alignment data. The 20% tolerance was added to the Q-value due to the microfabrication limitations of the MEMS devices.

Theta Adjust Stroke: The value of the theta adjust stroke was set to 70%, indicating that during theta alignment, the microscope of the dicing saw travels horizontally from left to right or vice versa over a distance equal to 70% of wafer's diameter.

The Spiral check Q-Margin: The spiral check Q-margin was set to 20% in the alignment data function screen; it provides a tolerance of 20% to the Q-level for spiral check verification during alignment teaching operation. The resultant Q-value of an appropriate target pattern should be less than the difference between the numerical values of the Q-level and the spiral check Q-margin.

In addition, the alignment teaching operation will automatically record the window size X, window size Y, direct light level, oblique light level, street adjustment, and hairline width. Figure 10 shows a screenshot of alignment data.

4.4. Workpiece loading

The dicing frame with a wafer was first placed on the chuck table of the dicing saw machine, as shown in figure 11. Due to the manual preparation of the wafer sample, the dicing streets (or cutting lines) were not aligned parallel to the dicing blade. Therefore, the tilt of the dicing streets will also be adjusted during the alignment teaching.

4.5. Low magnification (0.75X) rough theta alignment

The macro target window was opened using the 'F-Teach' option from the manual operations menu after the dicing saw was initialized. Optimal contrast between the features on the wafer was achieved by manipulating the intensity of direct and oblique lighting of the microscope. The light information was then saved by clicking the 'Enter' button. The focus of the microscope was then adjusted to the surface of the wafer using the 'Focus' button. The 'Exit' button was pushed in order to return to the macro target window.

The center of the green target window was first aligned with the edge of the dicing street on the left-hand side of the wafer, as showed in figure 12. Upon clicking the 'Align-θ' button, the microscope traveled to the right side of the wafer, covering a distance equivalent to 70% of the wafer diameter. Next, the center of the green target window was aligned parallel to the edge of the dicing street on the right side of the wafer. It is advised to repeat this operation many times until the center of the green target window aligns parallel to the edge of the dicing street.

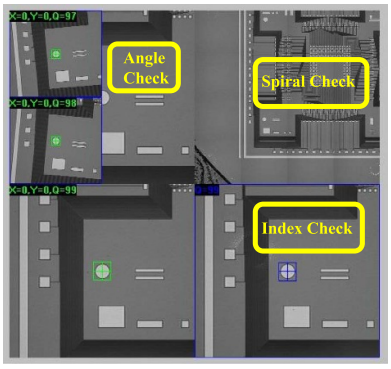

Figure 13. Q-value results of a good CH1 Macro target.

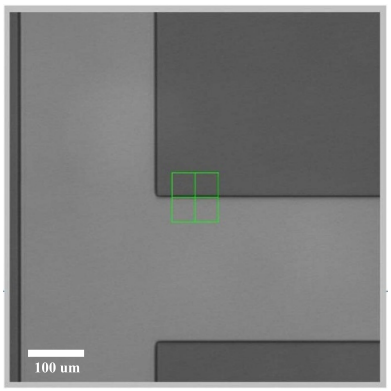

Figure 14. Screenshot of the dicing saw after the target window was aligned horizontally with the dicing street edge on the wafer at high magnification (7.5X).

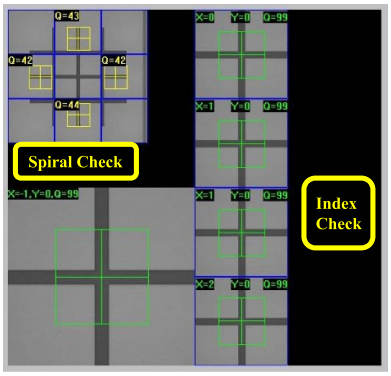

Figure 15. Q-value outcomes of a good CH1 Micro target.

4.6. Channel 1 macro target teaching

The microscope was again adjusted for illumination and focus to provide optimum contrast for the features on the wafer, as explained in the preceding section. The circle was enclosed inside the green target window as a macro target since only the window interior is considered a target. The dimensions of the target window concerning the size of the circle were adjusted using the 'ADJ-Window' function. The dicing saw machine performed spiral, angle, and index verification checks after pressing 'Enter' to determine whether the chosen macro target was appropriate. The dicing machine indicated in the information bar that the 'Target is good' based on the Q-value results of all three verification tests. The screenshot of the dicing saw in figure 13 shows the Q-values of an acceptable macro target. The macro target information was recorded by pressing the 'Enter' key. The macro target has to be taught again if the dicing machine determines that the selected target is incorrect.

4.7. High magnification (7.5X) fine theta alignment

The microscope's magnification automatically switches to higher magnification (7.5X) after entering the micro-target teaching screen. For precise tilt correction in the wafer, the fine theta alignment was repeated at high magnification, identical to the one done at low magnification in section 4.5. Figure 14 shows the green target window once its center is horizontally aligned with the edge of the dicing street.

4.8. Channel 1 micro target teaching

Once the fine theta alignment had been completed, the microscope's illumination and focus were adjusted for the optimum contrast of the features on the wafer. The addition symbol (+) from one of the MEMS device chips was enclosed inside the green target window as a micro-target. The 'ADJ-Window' function on the user interface was used to adjust the height and width of the target window according to the dimensions of the micro-target. The 'Enter' key was pressed after the selection of the micro-target to check whether the selected target was appropriate. The dicing saw conducted spiral and index verification checks and showed the result in the information bar as 'Target is good.' If the dicing saw determines that the micro-target is inaccurate, it is advisable to repeat the teaching process with another appropriate target. The screenshot of the dicing saw in figure 15 shows the Q-value outcomes of a good micro-target.

4.9. Channel 1 street adjustment

The 'Micro Street Adjust' screen appears automatically after recording the micro-target in channel 1. The hairline's dotted borders were aligned parallel with the edges of the dicing street to accurately measure the distance between the micro-target and the cutting line. The distance from the micro-target to the street was measured and used as the first reference for the cutting process. It is recommended to conduct street adjustments at the intersection of two dicing streets. To avoid the dicing saw from misidentifying other features as kerfs during kerf check, ensure that there are no identical patterns by moving in the X-direction. Figure 16 exemplifies a well-executed street adjustment.

4.10. Channel 2 micro target teaching and street adjustment

The wafer was rotated at an angle of 90 degrees (as recorded in device data) by the automated movement of the chuck table to reach the micro-target teaching window in channel 2. The hash

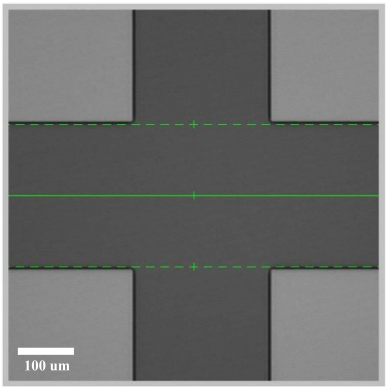

Figure 16. Hairline of a dicing saw aligned with the dicing street on the wafer in CH1.

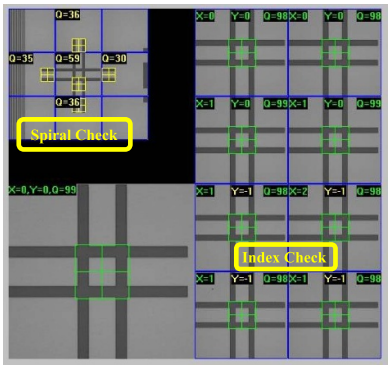

Figure 17. Q-value outcomes of a good CH2 Micro target.

symbol feature (#) was selected as a second unique micro-target for teaching operation. In CH2, the street adjustment and micro-target teaching followed the same steps as in CH1's teaching procedure. Please see sections 4.8 and 4.9 for reference. The screenshot of the dicing saw in figure 17 presents the Q-values of an acceptable micro-target.

Note: The alignment teaching in channels 1 and 2 is sufficient for square or rectangular MEMS devices. However, it is possible to teach alignment in channels 3 and 4 for hexagonal or octagonal devices.

4.11. Teaching data writing

When the teaching procedure on macro and micro-target patterns was finished, the data was saved in the dicing saw by pressing the 'Enter' key. Figure 18 shows the recorded macro and micro targets.

4.12. Potential errors in alignment teaching and their troubleshooting

The alignment errors presented in this section were encountered during optimizing the alignment teaching procedure. Solutions to these potential errors are explained herein.

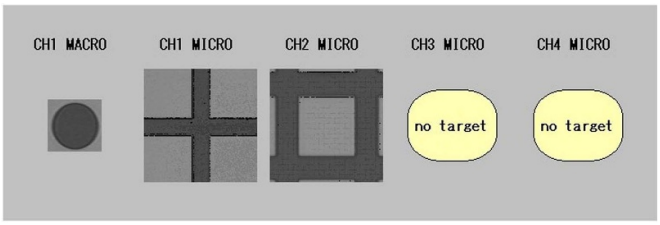

Figure 18. Screenshot of the dicing saw showing 1 Macro and 2 Micro targets recorded during alignment teaching operation.

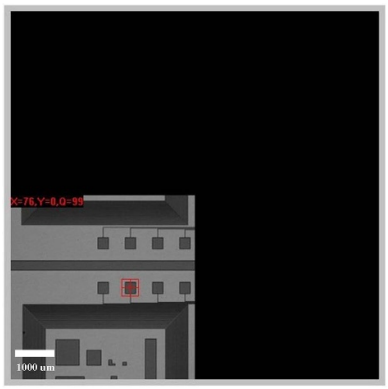

Figure 19. Screenshot of the dicing saw showing a rejected target pattern due to the presence of similar features nearby on the pseudo-MEMS chip of the wafer.

4.12.1. Wrong target selection. If the target verification procedure detects a comparable target (or feature) near the chosen target, the dicing saw will show an error message stating, 'Target is not good.' The chosen target in figure 19 had a 99% similarity to a neighboring feature. This error may occur if the selection window does not have a target.

Solution: Selecting a unique target pattern that does not resemble any structure on the chip can fix this issue.

4.12.2. Index-check error. Index error occurs when the index value recorded in the dicing saw—the distance between the centers of two successive dicing streets—does not match the actual index value on the wafer. Consequently, the dicing saw terminates the alignment teaching operation with the error message 'Index check is not good.'

Solution: The 'Measure' function can determine the real and precise index values on the wafer. The revised index values will rectify the index error.

4.12.3. Error due to fabrication defects. Fabrication flaws are mostly inevitable in a multi-user cleanroom facility, and these inaccuracies may be in the form of missing features or unwanted particles in different locations of the wafer. If the manufacturing defects are located on or near the target patterns, alignment errors might occur as a result of target misrecognition by the dicing saw. In figure 20, the manufacturing defects can be seen around the features.

Solution: To prevent the misrecognition of targets during dicing, it is advisable to use a combination of direct and

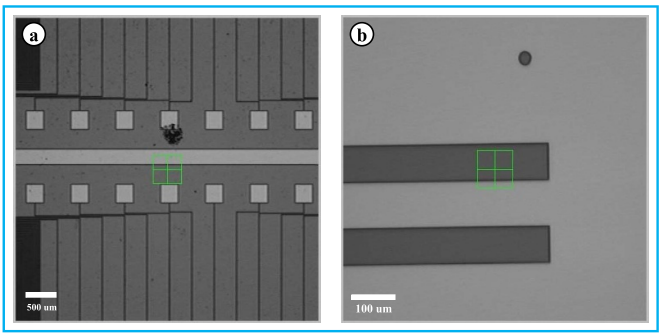

Figure 20. Microfabrication defects on the pseudo-MEMS chips of the wafer: (a) Undeveloped photoresist feature, (b) A cluster of unwanted particles.

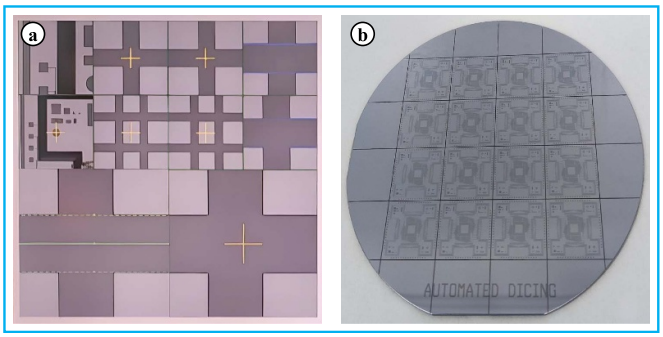

Figure 21. Fully Automated Dicing of a 4 inch diameter Silicon wafer: (a) Screenshot of dicing saw user interface showing detected macro and micro targets on the wafer after successful auto-alignment, (b) Image of the wafer after it has been diced successfully into 16 pseudo-MEMS device chips.

oblique illumination to achieve the optimal contrast of the features on the substrate. Selecting a defect-free target is an alternative approach to address this problem.

5. Fully automated dicing operation

Alignment teaching is a pre-requisite for the complete automation of the dicing saw operation. The dicing saw readies itself for automated dicing after the successful alignment teaching procedure. A single touch of the 'Start' button in the 'Full-Automation' user interface initiated a two-channel automated dicing process. No further support was needed for the dicing after this stage. The dicing saw performed an automatic alignment and then diced the wafer into square pseudo-MEMS device chips. Figure 21(a) shows the screenshot of the dicing saw user interface after auto-aligning a 4 inch silicon wafer. An image of the wafer is shown in figure 21(b) after it has been successfully diced into chips by a fully automated dicing process.

6. Dicing saw processing time

A dicing time simulator based on analytical formulations to calculate the total dicing saw processing time for a given wafer (Please see chapter 6, section 6.3, equation (6.1), and table 6.2 in [26]) is developed. Dicing time simulator calculations of dicing saw processing time do not exactly match but are close to the experimental time. Although it is easy to adapt to equation (6.1) in [26], the dicing time simulator does not consider additional cut length as a result of the machine tolerance value for cut clearance of the dicing blade. The dicing time simulator does not provide the details of turnover time; instead, it gives an approximate turnover time for each cut, while in reality, the turnover time strongly depends on where the dicing line is positioned compared to the centerline of the wafer under dicing saw processing. Furthermore, the simulator does not account for additional time (consumed by the dicing saw) if the wafer is cut in multiple depth steps instead of a single deep cut. Moreover, a patent study presents an analytical approach for the calculation of the wafer-cutting time by calculating the total cutting length of the wafer [27]. Nonetheless, the total cutting-length formulae provided in the patent do not take into account the turnover time from one dicing line to the next dicing line. Furthermore, extra dicing processing time and extra turnover time on the same cutting line, when the wafer is diced in multiple depth steps instead of a single cut, is not taken into account. Hence, we developed a comprehensive analytical formulation that includes turnover time and additional time required for multi-step cutting for the accurate calculations of dicing saw processing time for the manufactured wafers.

The overall time duration of the dicing process consists of the following components: the cutting time for the dicing blade (T_1), the time used for the chuck table to return during multi-step cutting (T_2), the time required for the chuck table for line switching (T_3), the time needed for the chuck table for channel switching (T_4), and finally the time taken for the blade to ascend and descend before and after completing a cut (T_5).

$$T_{\text{total}} = T_1 + T_2 + T_3 + T_4 + T_5 \tag{1}$$

6.1. Cutting time (T_1)

Cutting time is defined as the time when the dicing blade touches the substrate and cutting is being performed. Equation (2) is the general expression to calculate the time of basic machining processes, such as drilling, turning, and milling [30].

$$T = \frac{L}{F} \tag{2}$$

where T is the cutting time in seconds, L is the total cutting length in millimeters, and F is the feed rate in millimeters per second.

The blade holder remains stationary while the blade rotates at a specified RPM during the dicing process. Moreover, the chuck table travels towards the blade holder while carrying a substrate that is mounted and is meant to be cut into chips. Equation (2) could also calculate the cutting time of a dicing

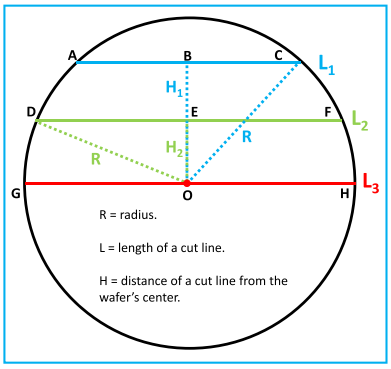

Figure 22. Schematic of the wafer for cutting length calculations (not drawn to scale).

experiment by introducing another parameter, step cutting (S), which specifies whether the wafer was cut across its thickness in a single step or multiple steps. Equation (3) is used for calculating the time of the cutting process performed by the dicing saw.

$$T_1 = S \cdot \left(\frac{L_{\text{total}}}{F}\right). \tag{3}$$

Total cutting length (L_{total}): It is defined as the distance between the centers of the dicing blade at the beginning and end of a cut line. In the given case, the wafer was diced by only three cut lines starting from the wafer's top edge. Schematic of the wafer with a center O and a diameter GH (equivalent to the length of the cut line L_3) is shown in figure 22. The L_1 and L_2 cutting lengths were determined using the Pythagorean theorem for triangle BCO and triangle DEO, respectively, and the derivation of the expressions is shown in equations (4) through (8). The general formula for the length of a single cut line on a wafer is given in equation (9). Equation (10) shows the mathematical expression for the entire cutting length of the wafer for a single cutting channel.

$$(R)^2 = (H_1)^2 + \left(\frac{L_1}{2}\right)^2 = H_1^2 + \frac{L_1^2}{4} = \frac{\left(4H_1^2 + L_1^2\right)}{4} \tag{4}$$

$$4R^2 = 4H_1^2 + L_1^2 \tag{5}$$

$$L_1^2 = 4\left(R^2 - H_1^2\right) \tag{6}$$

$$L_1 = 2\sqrt{R^2 - H_1^2}. \tag{7}$$

Similarly,

$$L_2 = 2\sqrt{R^2 - H_2^2}. \tag{8}$$

Hence, the general formula for the length of a cut line on the wafer:

$$L_n = 2\sqrt{R^2 - H_n^2}. \tag{9}$$

The total cutting length of the wafer in a single cutting channel:

$$L_{\text{total}} = 2\left(\sum_{n=1}^{k}\sqrt{R^2 - H_n^2}\right). \tag{10}$$

Equation (11) provides the revised equation for the cutting time with the addition of the cutting length formulation, and it holds for the wafer containing chips with different edge dimensions.

$$T_1 = \left(\frac{2.S}{F}\right) \cdot \sum_{n=1}^{k}\sqrt{R^2 - H_n^2} \tag{11}$$

where S stands for the number of cutting depth steps taken for a cut line, F represents the feed rate, k represents the total number of cutting lines for the whole wafer, starting from the wafer's top side to the wafer's bottom side (or vice versa), R is the radius of the wafer, and H is the distance of a cut line from the wafer's center.

6.2. *Chuck table return time in multi-step cutting (T_2)*

The thickness and mechanical properties of the wafer determine whether it can be diced in a single step or whether the cutting process has to be done in multiple repetitive depth steps. In multi-step cutting, the chuck table returns to its original position on the same cut line after the 1st step without performing any cutting. Once the first cutting phase is finished, the 2nd cutting step follows the same line at a given cut depth. The chuck table returns horizontally (along X-axis) at a speed different from the feed rate by covering the distance equivalent to the length of the line it diced during the previous step. No cutting takes place while the chuck table returns to its starting position. However, this increases the overall processing time for the dicing operation. The time required for the return of the dicing blade in multi-step cutting can be determined using equation (12).

$$T_2 = (S-1) \cdot \left(\frac{L_{\text{total}}}{C_x}\right). \tag{12}$$

The total distance travelled by the chuck table (equivalent to L_{total}) was calculated in the section 6.1; therefore, the equation (12) is expanded as follows:

$$T_2 = \left(\frac{2.(S-1)}{C_x}\right) \cdot \sum_{n=1}^{k}\sqrt{R^2 - H_n^2} \tag{13}$$

where S stands for the number of cutting depth steps taken for a cut line, C_x represents the chuck table's speed along the X-axis, k represents the total number of cutting lines for the whole wafer, starting from the wafer's top side to the wafer's bottom side (or vice versa), and H is the distance of a cut line from the wafer's center.

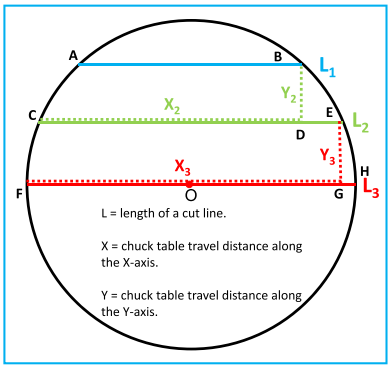

Figure 23. Schematic of the wafer for calculating line switching distance (not drawn to scale).

6.3. Line switching time (T_3)

The dicing saw consumes additional time when the chuck table positions the dicing blade from one cutting line to the subsequent cutting line. The chuck table first moves simultaneously along both the X-axis and Y-axis, but one of the two motions stops earlier than the other one depending on the wafer's diameter and edge dimensions of the chips to be diced. Hence, the time required by the chuck table to transit from point B to C or from point E to F in figure 23 is longer of the two times (X or Y components of the time) because the longer time 'absorbs' the shorter one. The time taken by the chuck table while traveling along the X-axis (T_{x_n}) and Y-axis (T_{y_n}) when transitioning from one cut line to another can be calculated by dividing the chuck table's travel distances along X and Y axes (X_n & Y_n) by their corresponding speeds (C_x & C_y), as shown in equations (14) and (15) (where index 'n' starts from 2).

$$T_{x_n} = \frac{X_n}{C_x} \tag{14}$$

$$T_{y_n} = \frac{Y_n}{C_y} \tag{15}$$

where X_n represents the distance traveled by the chuck table along the X-axis, C_x represents the chuck table's speed along the X-axis, Y_n is the chuck table's travel distance along the Y-axis (equivalent to edge dimensions of the chip or Y-index), and C_y represents the chuck table's speed along the Y-axis.

Chuck table's Line Switching Distances along X-axis and Y-axis (X_n & Y_n): figure 23 provides the schematic of the wafer. Distances X_2 (from point D to C) and X_3 (from point G to F) in figure 23 were estimated by summing the chuck table's horizontal distances while transitioning from L_1 to L_2 and L_2 to L_3 in the respective order. The derivation of mathematical expressions for distances X_2 and X_3 is shown by equations (16) through (18). Equation (19) is the generalized formulation for the distance X_n that the chuck table covers along the X-axis when switching from one line to another. Y_2 (from point B to D) and Y_3 (from point E to G) in figure 23 correspond to the distance the chuck table travels along the Y-axis while switching from L_1 to L_2 and L_2 to L_3, respectively. Chuck table's distance along the Y-axis (Y_n) corresponds to the edge dimensions of the chips to be diced.

$$X_2 = \frac{L_1}{2} + \frac{L_2}{2} \tag{16}$$

$$X_2 = \frac{L_1 + L_2}{2}. \tag{17}$$

Similarly,

$$X_3 = \frac{L_2 + L_3}{2}. \tag{18}$$

The generic formulation for the line switching distance X_n:

$$X_n = \frac{L_{n-1} + L_n}{2}. \tag{19}$$

The X and Y components of the time (T_{x_n} and T_{y_n}) for each line transition were compared, and the longer time was selected because it 'absorbs' the shorter time (if $T_{x_n} > T_{y_n}$ then $T_{y_n} = 0$, if $T_{y_n} > T_{x_n}$ then $T_{x_n} = 0$). Therefore, the total line switching time T_3 of the chuck table for the whole wafer in a single cutting channel is the sum of the individual line switching times, be it T_{x_n} or T_{y_n}, as shown in equation (20). Equation (20) takes into account the line transition time of chips with different edge dimensions (or Y-index values).

$$T_3 = \left(\sum_{n=2}^{k} T_{x_n} \text{ if } T_{x_n} > T_{y_n}\right) + \left(\sum_{n=2}^{k} T_{y_n} \text{ if } T_{y_n} > T_{x_n}\right) \tag{20}$$

where T_{x_n} and T_{y_n} represent the X and Y components of a line transition time, respectively, and k represents the total number of cutting lines for the whole wafer, starting from the wafer's top side to the wafer's bottom side (or vice versa).

6.4. Channel switching time (T_4)

The chuck table of the dicing saw rotates in order to transition between different cutting channels, depending on the geometry of the chips to be diced. The dicing saw consumes very little time (in comparison to T_1, T_2, and T_3) when switching channels. The channel switching time may be calculated by dividing the total angular distance (A_t) traveled by the chuck table by its angular speed (S_a), as shown in equation (21).

$$T_4 = \left(\frac{A_t}{S_a}\right). \tag{21}$$

6.5. Blade ascend and descend time (T_5)

The dicing blade descends from a certain height to the required depth on the substrate to start cutting, and it ascends to the same height after the cutting is completed. This time consumption during blade ascending and descending movements is too little, but it may become significant during multi-step cutting when it happens several times for each cut line. The time duration of the blade's movements along the Z-axis may be determined by dividing the distance it traveled (Z) by its speed (S_z),

as shown in equation (22). Equation (22) applies only to a single-step cutting process because it does not consider the blade's total ascend and descend distance in case of multi-step cutting.

$$T_5 = 2.k.\left(\frac{Z}{S_z}\right). \tag{22}$$

However, the Z value for the multi-step dicing would enlarge in each subsequent cutting step by a fixed depth of 'd' due to the corresponding increase in blade penetration into the substrate. Therefore, the total distance Z_t the blade traveled in multi-step cutting can be determined using Arithmetic Progression, as shown in equation (23). Equations (24) and (25) provide mathematical expressions for the time T_5, and that hold for both single-step and multi-step cutting processes:

$$Z_t = \frac{S.(Z_1 + Z_n)}{2} = \frac{S.(2Z_1 + (S-1)\,d)}{2} \tag{23}$$

$$T_5 = 2.k.\left(\frac{Z_t}{S_z}\right) \tag{24}$$

$$T_5 = \frac{k.S\ (2.Z_1 + (S-1)\,.d)}{S_z} \tag{25}$$

where k represents the total number of cutting lines for the whole wafer, starting from the wafer's top side to the wafer's bottom side (or vice versa), S stands for the number of depth steps for each cut line in multi-step cutting, Z_1 and Z_n are the cut depth during the first and last cutting steps of a cut line, respectively, and d is the common difference between two successive cut depths of a cut line.

6.6. Formulation of total dicing saw processing time

Equation (26) provides the final mathematical formulation for the overall processing time of the mechanical dicing saw.

$$T_{\text{total}} = T_1 + T_2 + T_3 + T_4 + T_5$$

$$\begin{aligned} T_{\text{total}} = {} & \left(\frac{4.S}{F}\right)\cdot\sum_{n=1}^{k}\sqrt{R^2 - H_n^2} \\ & + \left(\frac{4.(S-1)}{C_x}\right)\cdot\sum_{n=1}^{k}\sqrt{R^2 - H_n^2} \\ & + \left(\sum_{n=2}^{k} T_{x_n}\ \text{if}\ T_{x_n} > T_{y_n}\right) \\ & + \left(\sum_{n=2}^{k} T_{y_n}\ \text{if}\ T_{y_n} > T_{x_n}\right) \\ & + \left(\frac{A_t}{S_a}\right) + \left(\frac{k.S\ (2.Z_1 + (S-1)\,.d)}{S_z}\right) \end{aligned} \tag{26}$$

where S represents the number of depth steps for a cut line in multi-step cutting, F represents the feed rate, k represents the total number of cutting lines for the whole wafer, starting from the wafer's top side to the wafer's bottom side (or vice versa), R is the radius of the wafer, H is the distance of a cut line from the wafer's center, T_{x_n} and T_{y_n} represents the X and Y components of a line transition time, A_t is the total angular distance covered by the chuck table while transitioning between the cutting channels, (S_a) represents the angular or rotational speed of the chuck table, Z_1 is the cut depth during the first cutting step of a cut line, d is the common difference between two successive cut depths for a cut line, and (S_z) is the speed of the dicing blade along the Z-axis.

The DISCO DAD3220 dicing saw machine has a chuck table X-axis speed (C_x) of 500 mm s^{-1}, a chuck table Y-axis speed (C_y) of 200 mm s^{-1}, an angular chuck table speed (S_a) of 180 degrees s^{-1}, and a dicing blade Z-axis speed (S_z) of 50 mm s^{-1}. It is important to note that the speed values may vary depending on the specific version of the tool or the developed process recipe.

6.7. Comparing experimental and theoretical dicing times

A MATLAB code (given in the supplementary file) was developed using equation (26) to simulate the total dicing time for the one-step cutting process of a 4 inch wafer containing a 4 by 4 array of pseudo-MEMS device chips. The dimensions of the chips were measured at 17 mm × 17 mm, including the width of the dicing street. The calculated (or theoretical) processing time for the dicing saw was determined using MATLAB code, while the experimental time was measured using a stopwatch. Figure 24 shows that the experimental and calculated values were almost identical with a difference of less than 2 s, validating the formulated mathematical expression for the dicing saw processing time. This comparison did not consider the time required for auto-alignment, which is affected by the tool's focus configurations and the size of the wafer and chip to be diced.

Smaller samples measuring 3 mm × 3 mm, including the width of the dicing street, were also diced in multiple depth steps to ensure the formulation created for the dicing saw processing time was accurate. Figure 25 shows that the total experimental time for dicing trials with various depth steps was only about 1 s longer than the time calculated by the MATLAB code. This slight discrepancy between experimental and calculated dicing time values may be attributed to variations between the actual and input speeds of the dicing blade and chuck table. This time difference could become more

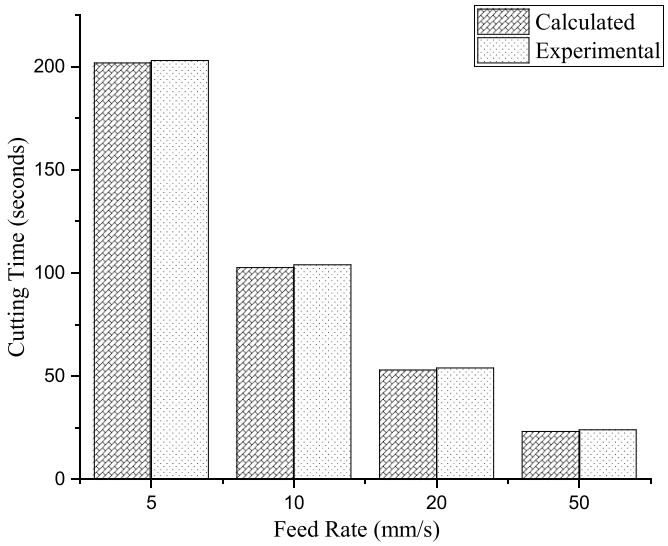

Figure 24. Comparison between the experimental and theoretical dicing saw processing times for a single-step cutting with 17 × 17 mm pseudo-MEMS devices of a 4 inch diameter wafer.

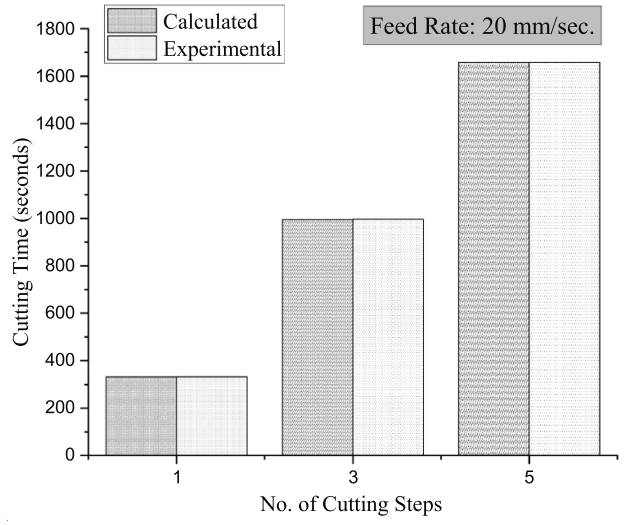

Figure 25. Comparison between the experimental and theoretical dicing saw processing times for a multi-step cutting of 3 × 3 mm chips of a 4 inch diameter wafer.

noticeable when cutting smaller samples in multiple depth increments. Speed calibration of the dicing saw's blade and chuck table can fix the difference in experimental and calculated dicing times. Human error is another possible factor since the stopwatch was manually started and stopped while recording the experimental dicing time.

7. Discussion

Selecting a unique alignment target is always crucial component for a successful alignment teaching process; it should bear minimum possible similarity to features nearby, or no similarity in the ideal case. The circle remained unaffected as a macro target, and the dicing machine could locate it easily during auto alignment, even though the circle rotated considerably around its axis while preparing the wafer for dicing. So, circles with various radii emerged as the most suitable macro target because they could pass all three verification tests during the alignment teaching trials. However, the dicing saw also declared only one rectangular target good out of 12 rectangular and square patterns. Therefore, this study recommends using circular features as appropriate macro targets.

All the potential micro targets, the hash symbol, the addition symbol, and the rectangle-pair showed promising results during alignment teaching trials. These micro-targets meet the definition of a suitable micro-target because they feature numerous straight lines in the *X*-direction (i.e. vertical lines) and at least one straight line in the *Y*-direction (i.e. horizontal line). The absence of straight lines in the *X*-direction affects the alignment accuracy. Consequently, the addition sign, rectangle-pair, and hash symbol were suggested to serve as appropriate micro targets for the alignment teaching procedure.

The alignment teaching procedure was successful regardless of whether the wafers were made of Pyrex or Silicon and the MEMS structures were manufactured from Photoresist or Copper. The key difference is that *Q*-values vary depending on the substrate material and material of the structures on MEMS devices. The maximum size of the target window-2.52 mm by 2.52 mm in low magnification mode and 0.332 mm by 0.332 mm in high magnification mode-limits the size of the macro and micro targets, respectively. This restriction ensures that alignment targets do not occupy excessive space. Additionally, the straight lines of a target should be at an appropriate distance from each other: the least distance between two lines should be 160 microns when the microscope is at low magnification (0.75X) and 16 microns when the microscope is at high magnification (7.5X). Therefore, the alignment targets can be made as small as possible considering the limitations imposed by the alignment teaching system of specific dicing saw machines.

Estimation of total dicing saw processing time is crucial in the semiconductor industry because it helps with optimizing chip production time. It provides accurate processing time that reduces idle time and improves the overall efficiency of the equipment. Moreover, the processing time may be determined using the developed analytical formulation even before executing the dicing process for wafers containing multiple devices (i.e. ranging from a few hundred to thousands). Once the engineers know the processing time, they do not have to monitor the dicing equipment continuously and can efficiently allocate the time for other tasks to enhance productivity.

8. Conclusion

We developed and implemented a completely automated dicing procedure to singulate MEMS chips from full-size

wafers. A systematic trial and error procedure identified the circle as the ideal macro target and the addition symbol, hash symbol, and rectangle pair as ideal micro targets from a pool of potential alignment targets for the alignment teaching operation. The optimized macro targets and micro targets were successfully recorded in the dicing machine during the alignment teaching work, and process errors were also troubleshooted. The developed process recipe enabled fully automated (i.e. only one-click to initiate and finalize the singulation process) dicing to separate MEMS devices from wafers safely and within estimated time range. Independent of the substrate material or materials used in the microfabrication, the alignment training assisted fully automated dicing may be designed and implemented for MEMS/NEMS devices. A DISCO dicing saw machine (DAD3220) was utilized to conduct the alignment teaching procedure that is detailed in this article. It is crucial to emphasize that this process may also be applied to other lab or industrial-scale dicing machines equipped with visual alignment systems. Finally, mathematical formulations were also created to estimate the total dicing saw processing time required to singulate MEMS/NEMS devices, and the calculated processing time closely approximates the experimental measurements.

Data availability statement

All data that support the findings of this study are included within the article (and any supplementary files).

Acknowledgments

We thank TUBITAK (Scientific and Technological Research Council of Turkey) for the financial assistance provided for this work under Project No. 118S041 of the 1003 Project Program. This work was performed at the National Nanotechnology Research Center (UNAM) at Bilkent University, supported by the Ministry of Industry and Technology of the Republic of Turkey within the scope of Law No. 6550 on the Support of Research Infrastructures.

ORCID iDs

Muhammad Rashid Mahmood https://orcid.org/0009-0000-5245-4598
Mehmet Yilmaz https://orcid.org/0000-0001-5496-6212

References

[1] Chang C *et al* 2014 Singulation for imaging ring arrays of capacitive micromachined ultrasonic transducers *J. Micromech. Microeng.* **24** 107002
[2] Lei W-S, Kumar A and Yalamanchili R 2012 Die singulation technologies for advanced packaging: a critical review *J. Vac. Sci. Technol.* B **30** 040801
[3] Young D J, Zorman C A and Mehregany M 2010 MEMS/NEMS devices and applications *Springer Handbook of Nanotechnology* pp 359–87
[4] Berman D and Krim J 2013 Surface science, MEMS and NEMS: progress and opportunities for surface science research performed on, or by, microdevices *Prog. Surf. Sci.* **88** 171–211
[5] Guenther T, Jiang Z X, Kim K and Sieloff D D 2009 Mesa sample preparation for secondary ion mass spectrometry depth profiling using an automated dicing saw *J. Vac. Sci. Technol.* B **27** 677–80
[6] Mei X, Patel N S, Bicen B and Khalsa S 2012 Automated optical inspection for die prep *ASMC Advanced Semiconductor Manufacturing Conf.) Proc.* pp 72–76
[7] Basu P K, Khanna A and Hameiri Z 2015 The effect of front pyramid heights on the efficiency of homogeneously textured inline-diffused screen-printed monocrystalline silicon wafer solar cells *Renew. Energy* **78** 590–8
[8] Richard Å, Rangsten P, Strandman C and Bäcklund Y 1999 Decreasing the optical path length in an optoelectronic module using silicon micromachining *J. Micromech. Microeng.* **9** 127
[9] Frommhold A, Manyam J, Palmer R E and Robinson A P G 2012 Fullerene-based spin-on-carbon hardmask *Microelectron. Eng.* **98** 552–5
[10] Frommhold A, Yang D X, McClelland A, Xue X, Palmer R E and Robinson A P G 2013 EUV lithography performance of negative-tone chemically amplified fullerene resist *Proc. SPIE* **8682** 86820Q
[11] Frommhold A *et al* 2015 Novel molecular resist for EUV and electron beam lithography *J. Photopolym. Sci. Technol.* **28** 537–40
[12] Frommhold A *et al* 2014 Optimization of fullerene-based negative tone chemically amplified fullerene resist for extreme ultraviolet lithography *Proc. SPIE* **9051** 905119
[13] Vesters Y *et al* 2018 Multi-trigger resist patterning with ASML NXE3300 EUV scanner *Proc. SPIE* **10583** 1058308
[14] Frommhold A *et al* 2013 Performance of negative tone chemically amplified fullerene resists in extreme ultraviolet lithography *J. Micro/Nanolith. MEMS MOEMS* **12** 033010
[15] Yang D X, Frommhold A, Xue X, Palmer R E and Robinson A P G 2014 Chemically amplified phenolic fullerene electron beam resist *J. Mater. Chem. C* **2** 1505–12
[16] Dawson G *et al* 2018 High-carbon fullerene based spin-on organic hardmask *Proc. SPIE* **10586** 74–83
[17] Yang D *et al* 2022 A fullerene-platinum complex for direct functional patterning of single metal atom-embedded carbon nanostructures *J. Phys. Chem. Lett.* **13** 1578–86
[18] Frommhold A, Palmer R E and Robinson A P G 2013 Spin-on carbon based on fullerene derivatives as hardmask materials for high-aspect-ratio etching *J. Micro/Nanolith. MEMS MOEMS* **12** 033003
[19] Popescu C *et al* 2017 Sensitivity enhancement of the high-resolution xMT multi-trigger resist for EUV lithography *Proc. SPIE* **10143** 186–94
[20] Popescu C *et al* 2018 Multi-trigger resist for electron beam and extreme ultraviolet lithography *Proc. SPIE* **10775** 1077502
[21] Popescu C *et al* 2017 Multi-trigger resist for electron beam lithography *Proc. SPIE* **10446** 1044608
[22] Popescu C *et al* 2018 Multi trigger resist for EUV lithography *J. Photopolym. Sci. Technol.* **31** 227–32
[23] O'Callaghan G *et al* 2019 Multi-trigger resist: novel synthesis improvements for high resolution EUV lithography *Proc. SPIE* **10960** 7–15
[24] Popescu C *et al* 2020 Performance enhancements with high opacity multi-trigger resist *Proc. SPIE* **11326** 175–84

[25] Robinson A P G *et al* 2018 High-resolution EUV lithography using a multi-trigger resist *Proc. SPIE* **10583** 367–76
[26] Lawes R 2014 *Mems Cost Analysis: From Laboratory to Industry* (CRC Press) pp 133–4
[27] Jin G *et al* 2017 Wafer cutting time calculation method and device *Chinese Patent* CN107180790B
[28] 2016 *Alignment Tips and Tricks* DISCO HI-TEC EUROPE GmbH
[29] Shi K W *et al* 2010 Investigations of the effects of blade type, dicing tape, blade preparation and process parameters on 55nm node low-k wafer *34th IEEE/CPMT Int. Electronic Manufacturing Technology Symp. (IEMT)* pp 1–6
[30] Creese R and Adithan M 1992 *Estimating and Costing for the Metal Manufacturing Industries* (CRC Press) pp 129–30